Settlement analysis using a generic ballasted track simulation package

Jou-Yi Shih[1], Ilaria Grossoni[2], Yann Bezin[2]

1: Birmingham Centre for Railway Research and Education, School of Civil Engineering, University of Birmingham, Birmingham, B15 2TT, UK

2: Institute of Railway Research, School of Computing and Engineering, University of Huddersfield, Huddersfield, HD1 3DH, UK

*: corresponding author; email: j.shih@bham.ac.uk

Abstract

Uneven track settlement inevitably occurs for ballasted track and eventually results in poor track geometry and support stiffness leading to considerably high maintenance cost. Considerable *in situ* and laboratory experiments have been carried out and empirical formulas have been proposed in order to predict track settlement. Nevertheless, laboratory tests are usually restricted in size for financial reasons and the site characteristics vary significantly to fully understand influential parameters. Therefore, the main aim of the present work is to develop an efficient model capable of replicating localised track settlement for different circumstances. A generic ballasted track simulation package BaTrack is introduced combining the Finite Element (FE) software Abaqus, Python, and Fortran. The three-dimensional (3D) FE model includes rail, sleepers, rail-pads, under sleeper pads (USPs), ballast and foundation layers. An advanced non-linear ballast material model is introduced using porous material properties and extended Drucker-Prager model with hardening and is able to account for different confining pressure values. The model is firstly used for comparison against a series of monotonic triaxial tests and has shown good agreement. It is then validated against a series of full size tests carried out at the Southampton Railway Testing Facility (SRTF). A number of settlement analyses are carried out and characteristics of the stress, contact pressure distribution and void evolution from different track configurations are discussed in detail.

Keywords: Ballasted track, Finite Element (FE), porous material, Drucker-Prager, elasto-plastic material, settlement, triaxial test

1. Introduction

In continuous use for nearly 200 years, ballasted track remains widely used due to its relatively low cost of construction and well understood and controlled maintenance process. The main function of the ballast is to resist vertical, lateral and longitudinal vehicle loads and spread them out from the sleepers to the lower layers. In addition to that, it helps maintain the superstructure original geometry and provides resilience to the whole track system as well as absorption of noise and vibrations. It also provides fast drainage as it is a draining coarse aggregate. However, ballast degradation results in track geometry loss and possible hanging sleepers, which is a very common and detrimental phenomenon that tends to be exacerbated by the requirement for increasing speed and load as well as higher infrastructure capacity [1–3].

In order to have a better understanding of the fundamental characteristics of ballast behaviour, a large number of triaxial test results can be found in the literature (for example, see [4–11]). The monotonic tests show that the ballast material has a highly pressure dependent behaviour. An increment of resilient modulus as well as the initial yield stress and hardening stress can be found with increasing confining pressure. In contrast, the dilation angle decreases when confining pressure increases. This is due to the increased contact surface leading to higher stiffness and material strength with higher applied pressure. The cyclic tests show the increase of resilient modulus and density with the number of loading cycles. This can be explained with the fact that the ballast is more and more compacted resulting in higher stiffness. Furthermore, ballast breakage might occur when a large number of loading cycles is applied and that may accelerate ballast degradation. The size of the aggregate as well as the void ratio reduces, which theoretically results in higher dry mass density of the ballast. However, the stiffness of the ballast and settlement rate will eventually reach an approximately constant value after a certain number of repeated loads. The Poisson's ratio of the ballast marginally increases with the number of cycle. However, a constant ratio is usually derived after a certain loading cycles [9,10].

Although the characteristics of the ballast behaviour can be obtained from the triaxial tests, the settlement results are not very representative. This is due to the fact that only a constant confining pressure can be applied during triaxial test, which is not the in-situ ballasted track condition, where the horizontal stresses vary along the ballast depth and continuously changes with the passage of the load over consecutive sleepers. Furthermore, influences of the superstructure cannot be considered during triaxial tests. The distribution of pressure also changes with track components such as sleeper and rail types. In order to capture the behaviour of ballast track more appropriately, various laboratory facilities reproducing a section of track have been introduced [12–17]. Nottingham rail testing facility [12], the GRAFT facility in Edinburgh [15] and PSPTA rig in Wollongong [16] all include three sleepers and two rails, while the Southampton Railway Testing Facility (SRTF) [13,14] one sleeper with boundaries that are able to replicate the confinement from the adjacent sleepers. The Cedex Track Box [17] is a 21 m long, 5 m wide and 4 m deep complete facility, including sleepers, rails and fastening systems. Similar test rig was carried out in China for investing the track settlement in the high-speed railway [18]. However, the cost of such facilities can be high and compromises are often made by having to reduce the representative size of the experimental rigs and the representative range of applied loads.

In order to reduce the experimental costs and be able to explore various track configurations, a number of numerical approaches have been introduced to model ballasted track either using discrete element methods (DEM) or a continuum approach (FEM). DEM modelling has been shown to be able to satisfactorily capture the granular ballast behaviour. For example, research carried out in Nottingham [19–21] shows that considering sphere clumps gives a more realistic response in terms of load-deformation curve due to the interlocking mechanism. Monotonic and cyclic triaxial tests have been simulated using a range of confining pressure and compared with experimental data with a good agreement achieved, highlighting the importance of consider asperities. In addition, the work carried out by Harkness *et al.* [22] demonstrates the importance of surface roughness that is modelled using

friction coefficient as function of the normalised load, on monotonic and cyclic triaxial tests. A more complex DEM model with consideration of geogrid was carried out by Ngo *et al.* [23]. The results were compared with lab measurement and good agreement was found.

However, DEM models remain computationally very demanding. Thus, the continuum approach used in FE models has been commonly used to obtain the characteristic stress distribution of more representative track sections. For example, an elasto-plastic constitutive model for coarse granular aggregate ballast, which considered the degradation of particles due to shearing and incorporates the particle breakage, was proposed by Salim and Indraratna [24]. The model was based on the ratio between the deviatoric and mean stresses as a function of dilatancy, strength and particle breakage. Due to the fact that the resilience is related to the number of load cycles, a cyclic densification model was then proposed by Indraratna *et al.* [25]. Another elasto-plastic multi-mechanism model that is based on a Coulomb-type failure criterion and the concept of critical state is proposed by Aubry *et al.* [26]. Good agreement were found compared to triaxial tests ([24,25,27]). In Suiker and Borst [28], a two-dimensional (2D) full-track model has been developed and compared to the in situ track measurement based on a validated monotonic triaxial test modelling. This model is a purely mechanical approach, which avoids using empirical laws to associate the long-term behaviour. However, this model is developed on the basis of axisymmetric stress conditions. It is limited to two-dimensional problems and cannot be applied directly to dynamic problems [29]. A 2D full-track model using Hardening-Soil (HS) model combined with hypo-elastic material for ballast was introduced in Indraratna *et al.* [30] and extended to three-dimensional (3D) by Kalliainen *et al.* [31]. Commercial FE software, such as Abaqus and Ansys, are commonly used due to their efficient solver and mesh generation even for a complex geometry. Although the material constitutive model is limited and cannot correctly model the ballast behaviour ([32,33]), a more detailed material constitutive law can be derived using user-subroutines in Fortran ([29,34,35]). The implementation of new material constitutive law is not only complicated but also computationally time consuming

due to data exchange between the FE software and Fortran ([34,36,37]). Furthermore, a high number of input parameter needs to be used requiring a several triaxial tests and making it difficult to control the ballast behaviour [24–26].

The aim of the present work is to introduce a generic ballasted track model in a parametric environment that is able to capture the ballasted track mechanical behaviour and settlement characteristics. A generic ballasted track simulation package BaTrack, which combines a FE software Abaqus, Python, and Fortran, has been developed. The FE model is based on ballast characteristics found in literature and is able to account for different confining pressure corresponding to different constructions and loading cases. The results have been compared with a series of monotonic triaxial tests and full size tests carried out at the SRTF and have shown excellent performance in terms of accuracy and efficiency. A number of parametric studies have been carried out to investigate the effect of the number of sleepers considered, the ballast geometry, the presence of Under Sleeper Pads (USP) of varying modulus, geometry and material properties for each superstructure components and, finally, traffic loading characteristics.

2. FE ballast model

Firstly, an nonlinear elasto-plastic constitutive model for ballast material for individually applied confining pressure is developed and compared with published monotonic triaxial test results. It is, then, integrated into a generic model that can account for different applied confining pressure up to 115 kPa. Fresh ballast with grading according to the NR Standard RT/CE/S/006 Issue 3 is used here as an example.

2.1 Non-linar elasto-plastic constitutive model

Porous material properties are used for the elastic part and implemented in the commercial software Abaqus [38]. Experimental evidence suggests that during elastic straining in granular materials the change in the void ratio, e, and the change in the logarithm of equivalent pressure stress, p, are linearly related. As a result, the deviatoric elastic stiffness increases with increasing effective mean stress, p.

The deviatoric elastic behaviour can be defined either by choosing a given shear modulus or a given Poisson's ratio in Abaqus [38]. In order to consider the elastic shear stiffness increase as the material is compacted, a given Poisson's ratio is chosen here which allows the variation of deviatoric stress $d\mathbf{q}$:

$$d\mathbf{q} = 2\hat{G}d\mathbf{e}^{el} \quad (1)$$

where $\hat{G}$ is the instantaneous shear modulus, which is defined by the mean effective stress p, the instantaneous logarithmic bulk modulus κ, Poisson's ratio v, initial void ratio e_0, the tensile strength p_t^{el}, and volumetric strain ε_{vol}^{el}:

$$\hat{G} = \frac{3(1-2v)(1+e_0)}{2(1+v)\kappa}\left(p + p_t^{el}\right)\exp\varepsilon_{vol}^{el} \quad (2)$$

Here p_t^{el} is assumed to be zero because ballast is non-tension material.

As mentioned above, ballast shows a highly pressure-dependent behaviour. Therefore, the extended Drucker-Prager model [38] has been used in order to capture the frictional material which exhibit pressure-dependent yield (i.e. the material becomes stronger as the pressure increase). This model has been commonly used for simulating ballast behaviour [33,39]. Linear Drucker-Prager model is used in Abaqus by general exponent with b equal to 1 to define the yield surface:

$$F = aq^b - p - p_t = 0 \quad (3)$$

where a is a material parameter that is independent of plastic deformation and is constant with respect to deviatoric stress, q; p_t is the hardening parameter that represents the hydrostatic tension strength of the material and is determined by:

$$p_t = a\sigma_c - \frac{\sigma_c}{3} \quad (4)$$

where σ_c is defined by the uniaxial compression test. Due to the fact that the calibration data is obtained from the triaxial test, each applied confining pressure is then applied in order to obtain the correct hardening parameters.

This linear model provides for a possibly noncircular yield surface in the deviatoric plane to match different yield value in triaxial tension and compression, associated inelastic flow in the deviatoric plane, dilation (ψ) and friction (ϕ) angles. Instead of perfect plasticity, isotropic hardening is considered in order to have better agreement with the measurements. The hardening curve is defined by yield stress and absolute plastic strain without rate-dependency. Similar approach can be found in previous research performed by Shi, 2009 [10].

Triaxial test modelling is then carried out using a three-dimensional quarter of material sample. Confining pressure is applied surrounding the cylinder surface. Geostatic step is used to derive stable initial condition before applying vertical displacement in the z direction. A more detailed procedure can be found in Shih, 2017 [37]. The parameters listed in Table 1 are calibrated based on deviatoric stress and effective mean stress with different confining pressure during the monotonic triaxial test carried out by Shi, 2009 [10] and Aingaran [11]. In this paper, the same initial void ratio and mass density are used. Although void ratio decreases with increasing confining pressure, void ratio varies slightly during monotonic triaxial test [9,40]. Variation of void change is mainly due to particle breakage, which is not considered in the present model. On the other hand, the stiffness of the ballast changes significantly with different confining pressure. Therefore, the reference logarithmic bulk modulus has been changed slightly in order to account for this behaviour.

Here the mechanical behaviour within the elastic region is controlled by the instantaneous shear modulus and the instantaneous logarithmic bulk modulus. Although Poisson's ratio changes with different confining pressure [9,10], it is mainly dominated by the amplitude of applied load instead of the confining pressure [41]. Therefore, a constant Poisson's ratio is used to determine the reference

configuration and behaviour of swelling and compression is achieved by variation of logarithmic bulk modulus. Consequently, shear modulus changes (see Eq. (2)).

Table 1. Input parameters for the triaxial test modelling with different confining pressure values.

Confining pressure	5 kPa	10 kPa	30 kPa	60 kPa	115 kPa
Porous elastic material					
Logarithmic bulk modulus, κ	0.002	0.002	0.004	0.008	0.008
Poisson's ratio, ν	0.3	0.3	0.3	0.3	0.3
Tensile limit, p_t^{el}	0	0	0	0	0
Extended Drucker-Prager plasticity					
a	0.93	0.93	0.93	0.93	0.93
b	1	1	1	1	1
p_t	9.23	9.23	9.23	9.23	9.23
Dilation angle, ψ	30	30	25	25	20
Initial yield stress (kPa)	15	18	43	80	124
Initial void ratio, e_0	0.75	0.75	0.75	0.75	0.75
Mass density, ρ (kg/m^3)	1560	1560	1560	1560	1560

Good agreement can be found not only for stress-strain but also swelling behaviour compared with a series of monotonic triaxial tests found in the literature as shown in Fig. 1. As shown in Fig. 1(b), the results with higher confining pressure are more prone to compress at the lower strain level (i.e. lower than about 0.03). Therefore, a higher logarithmic bulk modulus, which allows more space for the model to compact, is given in order to have a better agreement with the results from laboratory tests. Poor agreement is found when axial strain is higher than 0.1 for the results with low confining pressure (i.e. 5 kPa and 10 kPa). This is due to the fact that the steady state has been reached for these two cases. A constant volumetric strain is obtained with increasing shear stress. Therefore, a constant dilation angle will not be able to predict particle behaviour correctly. However, the difference is still acceptable for strain range up to 0.12.

In summary, the model has the ability to accurately represent the ballast behaviour. Furthermore, parameters for the current elasto-plastic constitutive model are mainly the same for different confining pressure except for the logarithmic bulk modulus, the dilation angle and the hardening

curve, as shown in Table 1. Specific parameters are required for different confining pressure values. However, in reality the confining pressure, which represents the horizontal stress in the ballast layer, varies with depth and horizontal position in terms of different ballast geometry and applied loading (i.e. gravity load from track component and axle load). A generic constitutive model is then developed in order to detect the confining pressure and assign the appropriate parameters (see Section 2.2).

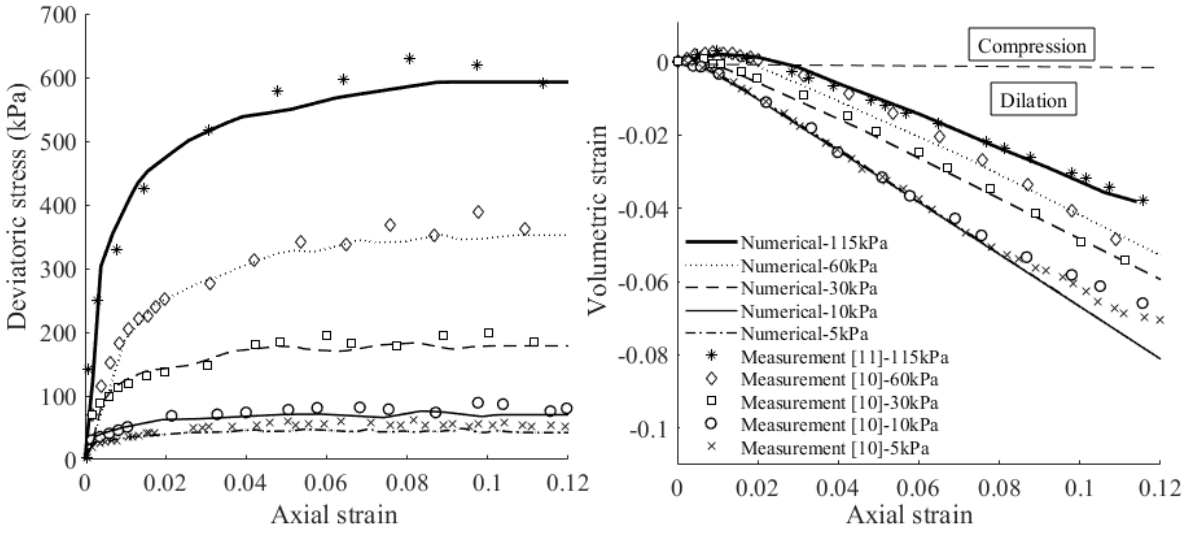

(a) (b)

Fig. 1. Comparison between numerical results from the present model and measurements with different confining pressure values [10,11]; (a) axial strain against deviatoric stress; (b) axial strain against volumetric strain.

2.2 A generic elasto-plastic constitutive model

A generic elasto-plastic constitutive model is introduced hereafter based on the elasto-plastic criteria explained in Section 2; however, with definition of stress dependent parameters in the existing constitute model. Thus, it can then correctly model the ballast material without the need for changing parameters manually while different confining pressures are applied. Instead of developing a new material constitutive model, which is complex and increases the simulation time due to data exchange and reconstruction of the material constitutive matrix, a user subroutine USDFLD has been established in order to calculate the relevant hardening curve, logarithmic bulk modulus and dilation angle for varying confining pressure during simulation. Data based on five different confining

pressure values (5 kPa, 10 kPa, 30 kPa, 60 kPa and 115 kPa) calibrated using test results available in the literature mentioned in Section 2.1 are used as reference input and linear interpolation is applied between data points in the tabular input in the USDFLD subroutine.

In order to show the strength of the present model, experimental data carried out by different researchers using different confining pressure values [11] are compared with the numerical results derived from the present model and good agreement is found, as shown in Fig. 2. This is especially true for the stress-strain curve (see Fig. 2(a)), with an average difference of 3.5% over the four confining pressure values considered. Higher differences are found in the axial strain-volumetric strain curve, as shown in Fig. 2(b). It is worth mentioning the difficulties of controlling the different initial condition applied in different laboratories. Different experimental results may be obtained due to slightly different initial conditions. However, the present model is able to capture the general behaviours appropriately and the differences are within acceptable range.

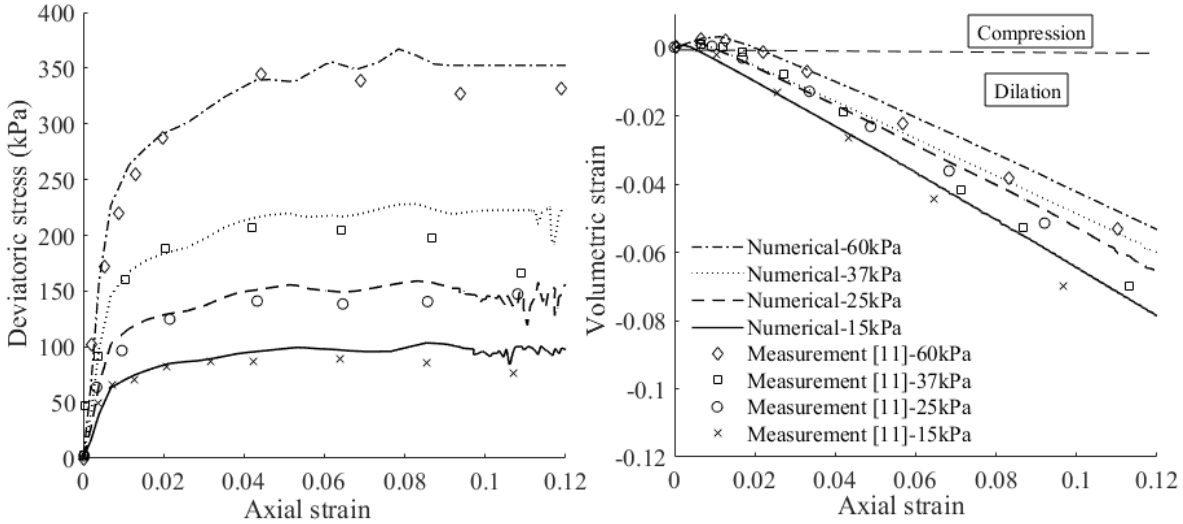

(a) (b)

Fig. 2. Comparison between numerical results from the present model and measurement with different confining pressure values [11]; (a) axial strain against deviatoric stress; (b) axial strain against volumetric strain.

3. The generic ballasted track simulation package BaTrack

The generic ballast track simulation package BaTrack is introduced here using a combination of Abaqus, Python and Fortran and providing parametric environment for settlement analysis. A 3D FE ballasted track model with consideration of superstructure and ballast elasto-plastic characteristics has been developed in BaTrack, which provides automated model generation (including model geometry, mesh strategy approach, analysis steps, contact and constraint setup, periodic boundary condition, initial condition and material), simulation, data acquisition, and data post-processing for different scenarios.

3.1 Model development

A 3D ballasted track model, which takes into account the superstructure characteristics (rail, rail pad and sleeper and optional USPs), the ballast geometry (height and width) and material characteristics, is shown in Fig. 3. Symmetrical loading is assumed and only half track is modelled with constrained transversal displacements within the symmetrical plane (see Fig. 3). Subgrade layer is modelled as an elastic foundation with equivalent stiffness to hard clay material. The translations in the three directions are constrained at the bottom of the foundation layer. Periodic boundaries (see details in Wu *et al.* [42]) are used at both ends for ballast, subgrade and rail in order to reduce the boundary effects and increase the calculation efficiency.

The Timoshenko beam element (B21) is used to represent the rail and single spring-dashpot to represent rail-pads. The main characteristic for rail-pads in the vertical direction is the stiffness. Therefore, in order to replicate the load distributing through this layer efficiently and correctly, a single spring-dashpot is used. Eight-node brick elements (C3D8) are used for sleeper and USP and four-node tetrahedral elements (C3D4) are used for ballast and foundation layers in order to have a better mesh. Note that the USP is set up to be tied underneath the sleeper and a surface-to-surface contact is established between the USP lower surface and the ballast top surface. A fine mesh is required in order to allow the stress distribution to be gradual. A sensitivity analysis has been carried out and the maximum element size is assumed to be around 0.1 m, corresponding to 6 rail beam

elements in a 0.65 m sleeper spacing. Total element number in this model is 4,870 considering one sleeper, 13,539 considering three sleepers and 22,482 considering five sleepers. The materials for all the track components with the exception of the ballast layer are assumed to be linear elastic with assigned Young's modulus and Poisson's ratio.

The sleepers can be assumed to be fully or semi-embedded within the ballast layer and the sleeper/ballast contact model, which is a surface-to-surface contact allowing separation, is set up between the bottom surface of sleeper and ballast layer in order to allow hanging sleepers to occur. Same contact model is applied between the side surface of sleeper and ballast layer. However, the friction, which is significant in the context of sleeper lateral resistant analysis [34], is not considered here as the main focus of this study is the vertical settlement and it would significantly increase simulation time without adding any extra information. In the present study the sleeper is set up to be fully embedded.

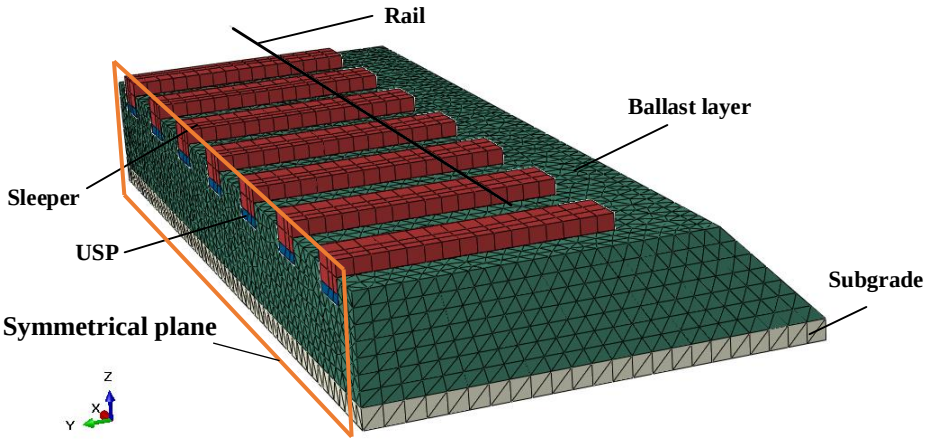

Fig. 3. 3D FE ballasted track model.

Each analysis consists of three steps (see Fig. 4). Firstly, the gravity load of the ballast is applied (geostatic analysis); secondly, the gravity load for sleepers and rail is considered (static analysis) and finally a cycle of loading and unloading of the point vertical load equivalent to a full axle is applied on top of the rail (static analysis) above the middle sleeper. Load variation that represents the loading

and the unloading cycle is defined through a given number of time steps. The inertia effects are neglected and the materials are time-independent. Furthermore, consideration of external horizontal force is not considered here due to the fact that the focus of the present study is the vertical settlement. Initial stress condition for the geostatic analysis is defined to be 0.54 kN/m^2 at the top of the ballast and the stress at the bottom of the ballast is calculated in terms of total weight of the ballast layer and the ballast bottom surface, e.g. 6.9 kN/m^2 for the case of one sleeper.

Although the user subroutine USDFLD can account for different confining pressure in triaxial test modelling, a modified code is required in order to account for variation of horizontal stress distribution in the ballasted track model. Unlike the triaxial test modelling where a constant horizontal stress can be obtained due to constant confining pressure applied in the x (longitudinal) and y (transversal) directions, the stress distribution may vary in the two directions for the ballasted track model. Furthermore, due to this inconstant stress value for each element at each time increment, the simulation suffers significantly to reach convergence especially for higher axle loads.

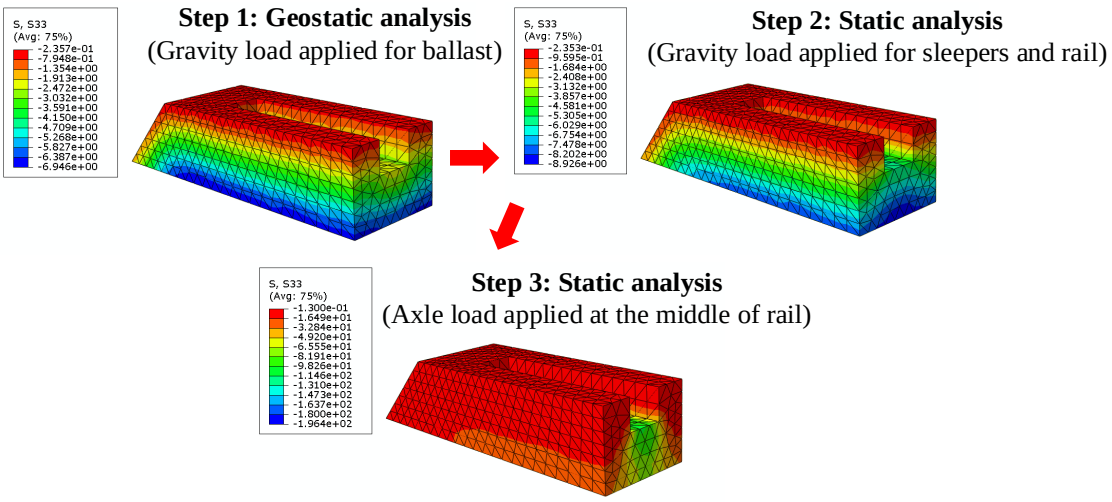

Fig. 4. Stress distribution along the vertical direction in three steps.

In order to solve the above issues, an additional UEXTERNALDB subroutine has been implemented to obtain the average stress level in a certain volume of the ballast layer and give the appropriate parameters at each time increment.

In the beginning of Step 1, the element information, including three-dimensional coordinates and element number, is extracted from the USDFLD subroutine in order to identify the average regions, which are defined by the number of the divided planes in three directions and the corresponding element numbers in the UEXTERNALDB subroutine. Stress level, S_i, for each i-th element is also outputted in the USDFLD subroutine and passed through the UEXTERNALDB subroutine after Step 1 for calculating the average stress level, $S_{avg,i}$, at *i* increment.

Two solution-dependent state variables, $S_{avg,j}$ and $\Delta S_{avg,j}$, (i.e. the average stress level at the current increment and the average variation of stress w.r.t. the previous time increment, respectively) are used for updating the appropriate parameters for the ballast material in the USDFLE subroutine. In order to obtain a more stable convergence, instead of updating the variable every time increment, the USDFLD user subroutine only updates the parameters when the difference between two average stress level $\Delta S_{avg,j}$, is higher than the previous calculated difference, $\Delta S_{avg,i}$.

The longitudinal stress is used as the convergence criteria and its value is averaged over the volume considered, which is the volume of ballast contained directly under each sleeper. This was the solution found to give the best agreement compared to the SRTF test (see Section 3.2) as well as best convergence and computational efficiency (see Section 3.3).

A detailed flow chart of the program is shown in Fig. 5, being T the value of total time at the beginning of the current increment.

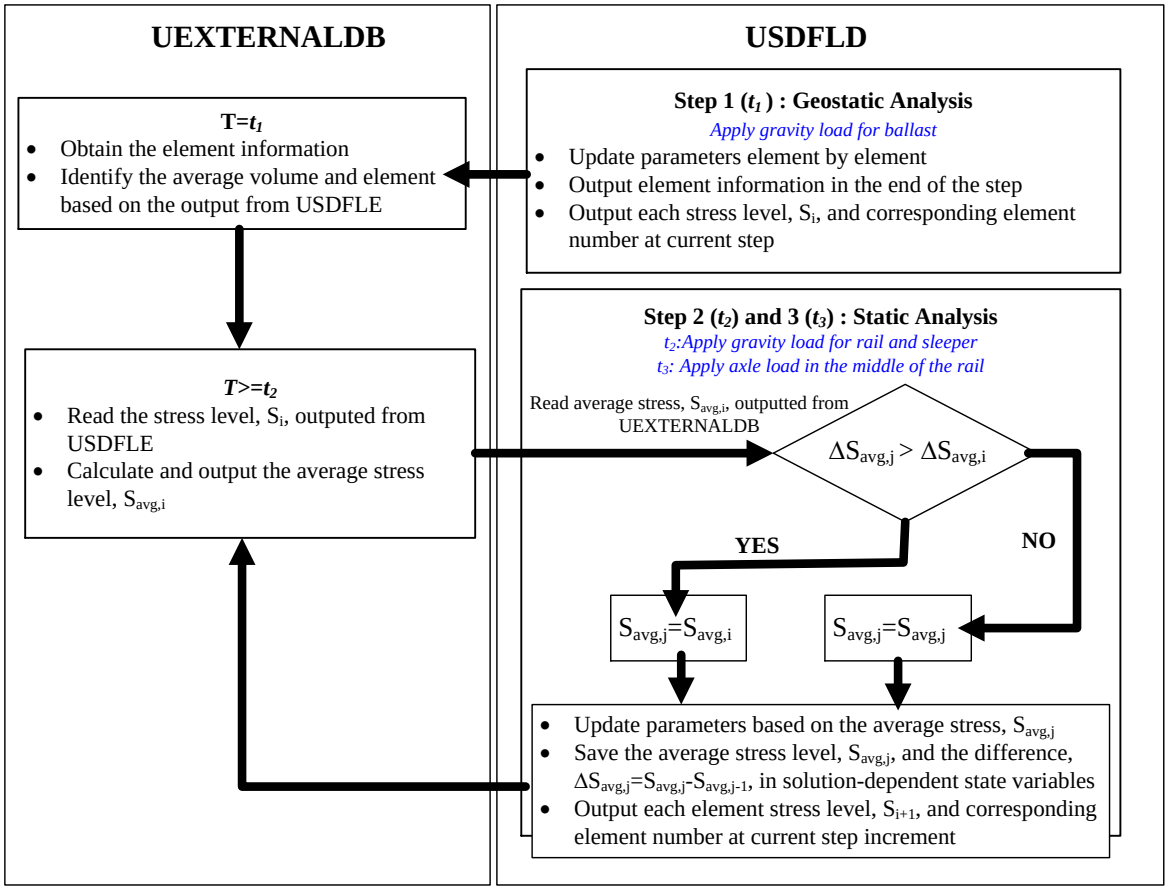

Fig. 5. Programming flow chart for the ballast material model.

3.2 Model comparison against laboratory tests

The FE ballasted track model results have been compared with the laboratory test data from the SRTF [43]. One sleeper is used and the main parameters used in the ballasted track model are listed in Table 3. Ballast material parameters can be found in Section 2. Note the height of ballast shoulder is not considered due to small influence observed for vertical settlement [34]. A 0.1 m thick foundation is used. The bottom of the foundation layer is fixed. An equivalent foundation Young's modulus equal to 80 MN/m^2 has been assigned in order to match the static deflection of the analytical results calculated using the elastic half-space theory for a given load and Poisson's ratio equal to 0.33.

Table 2. Parameters the ballasted track model.

Parameter	Value	Units
56E1-BS113A rail[1]		

[1] Note that the rail cross section is a generic beam section with the given area and second moment of area.

Rail mass density, ρ_r	7850	kg/m^3
Rail Young's modulus, E	2.1×10^8	kN/m^2
Rail Poisson's ratio, ν_r	0.3	
Rail area, A_r	0.007169	m^2
Rail second moment of area, I_{xx}	2.321×10^{-5}	m^4
Rail second moment of area, I_{yy}	4.216×10^{-6}	m^4
Rail shear constant	0.4	-
Rail-pad (Pandrol No. 45111, 2000)		
Rail-pad vertical stiffness, k_p	200×10^3	kN/m
G44 sleeper		
Young's modulus, E_s	5.70×10^7	kN/m^2
Poison's ratio, ν_s	0.2	-
Mass density, ρ_s	2688	kg/m^3
Sleeper height, h_s	0.2	m
Sleeper width, L_{sw}	0.24	m
Sleeper length, L_{sl}	2.5	m
Sleeper spacing, L_s	0.65	m
Additional parameters		
Rail gauge	1435	mm
Ballast shoulder width	0.6	m
Ballast layer depth	0.3	m
Ballast slope inclination	45	°
Foundation layer modulus	10.5×10^3	kPa

A detailed description of the SRTF laboratory test setup can be found in Le Pen [43]. 80 kN is the target total force to apply at the sleeper ballast interface and represents 50% of typical 15 t passenger axle load transferred to the sleeper directly below. A 5 kN dead load exists including the sleeper, rail and loading beam weight during the measurement. Therefore, the cyclic load from the hydraulic actuator was applied at the middle of the loading beam varying from 5 to 75 kN in order to obtain the total maximum force 80 kN and minimum force 10 kN. Due to the fact that here, only a half track model is considered and a loading beam is not included, the applied cyclic load is set up to vary from 3.2 kN to 38.2 kN within the gravity load from sleeper and rail.

The results are compared to the measurement data in terms of confining pressure and resilient deflection (deflection at the peak of one cycle and the deflection at the start of the following cycle) after one cycle. The mean confining pressure from four pressure plates (total area 1×0.3 m = 0.3 m^2)

is compared with the results from the FE model, as shown in Table 3. A very good agreement (less than 2% difference) has been found for cases of 10 kN and 80 kN.

Two resilient deflections were measured during the laboratory test at 0.1 m away from both sleeper ends: 1.33 mm and 0.48 mm, whose mean value is equal to 0.91 mm. The resilient deflection obtained at 0.1 m away from the sleeper ends from the FE model is 1.41 mm (i.e. difference of 55% w.r.t. the experimental results). The obtained difference is higher than the case of pressure comparison. This may be due to inappropriate alignment of the sleeper before the cyclic test or higher error may be obtained due to very small setup variation of the test. Nevertheless, the results from the present model are reasonably close to the measurement data.

Table 3. Confining pressure comparison between the FE results and test data from SRTF [43].

	Mean confining pressure (kPa)		
Load applied	FE model	SRTF	Difference
Initial 10 kN	4737.6	4738	0.01%
Initial 80 kN	14431.3	14195	1.7%

Stress distribution at every step considered are shown in Fig. 4. Higher stresses can be found at the bottom compared to the others due to higher gravity load from the ballast layer, sleeper and rail (see Fig. 4 Step 1 and 2). Although higher stress value is obtained at the boundary at Step 1, the stress distribution is almost uniformed for step 1 along the running direction, while a clear trapezoidal shape stress distribution can be found for step 3.

3.3 Investigation of the boundary effects

Although the periodic boundary condition has been applied to the two ends of the model, the model still requires a specific length in order to allow the stress to distribute correctly from the application point. An investigation on the minimum number of sleeper required is presented here in order to obtain a better understanding of the boundary effects. Settlement analysis is then carried out with applied load varying from 10 kN to 120 kN, which represents 2 to 24 t axle load approximately. The analysis follows the same procedure as presented before. However, the load is applied from 0 kN to

348 the maximum and then released to 0 kN again. The plastic settlement is then obtained by deducting
349 the final displacement value to the displacement value due to gravity load. The middle sleeper
350 displacement is used, and in this work it is assumed that the worst case scenario in terms of settlement
351 is when the load is directly above any one sleeper, i.e. highest sleeper to ballast pressure. Different
352 time increment for the third steps is used for different applied load. Higher axle loads require smaller
353 time increment in order to avoid convergence errors. Here 0.1 s is used for load up to 50 kN and 0.05
354 s is used up to 100 kN. Finally, 0.01 s and 0.001 s are used for 110 kN and 120 kN respectively.
355 The results using one, three and five sleepers can be seen in Fig. 6. Fig. 6(a) shows the plastic
356 settlement against the actual applied load at the sleeper level at the middle sleeper and Fig. 6(b) shows
357 the results against the contact force between sleeper and ballast. The results tend to converge with
358 more than three sleepers. The differences between the results from three and five sleepers are very
359 small, especially for low axle load. Higher differences can be observed when a larger axle load is
360 applied. Nevertheless, the difference is less than 5%. Same phenomenon can also be observed in
361 stress distribution when the maximum load is applied (120kN), as shown in Fig. 7. The stress
362 distributes mainly underneath the three central sleepers and much smaller stress energy can be found
363 in other areas. On the other hand, the results from one sleeper grossly overestimate the settlement
364 compared to the others. This is due to the restricted boundary at two ends that does not allow the
365 stress to distribute properly and eventually results in very high contact force between ballast and
366 sleeper, as shown in Fig. 6(b).
367 Although the model with three sleepers shows relatively good accuracy and efficiency, as shown in
368 Table 4, five sleepers are used for the further parametric study in order to avoid boundary interruption.
369 Note here seven or even more sleepers may be required for softer ballast and foundation stiffness due
370 to wider stress distribution. Nevertheless, the present parametric study does not consider variation of
371 foundation and ballast stiffness.

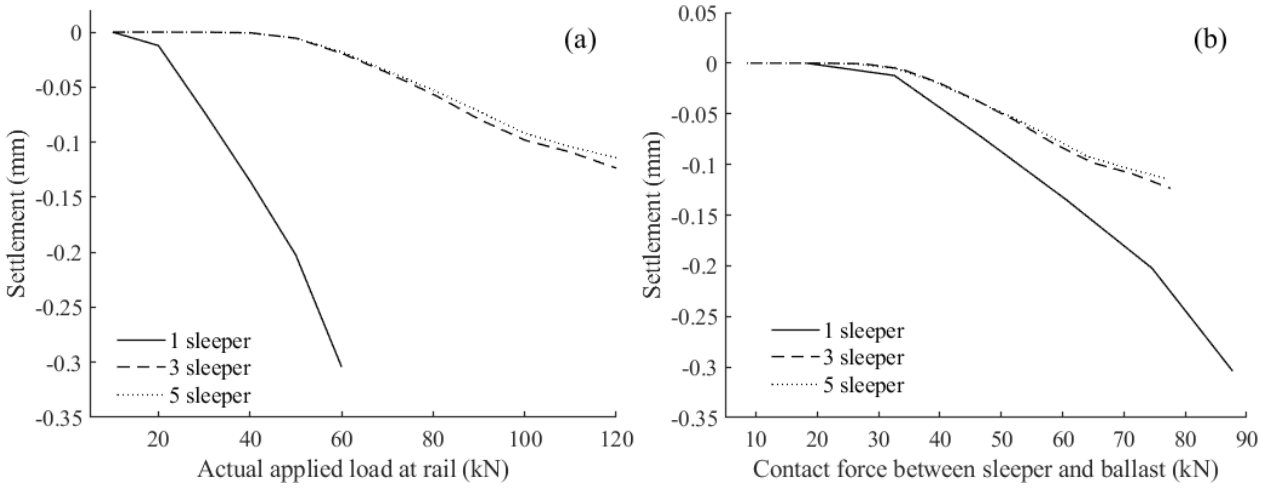

372

373 **Fig. 6.** Plastic settlement results at the middle sleeper from different sleeper number used; (a)

374 settlement against load at rail level; (b) settlement against load at sleeper level.

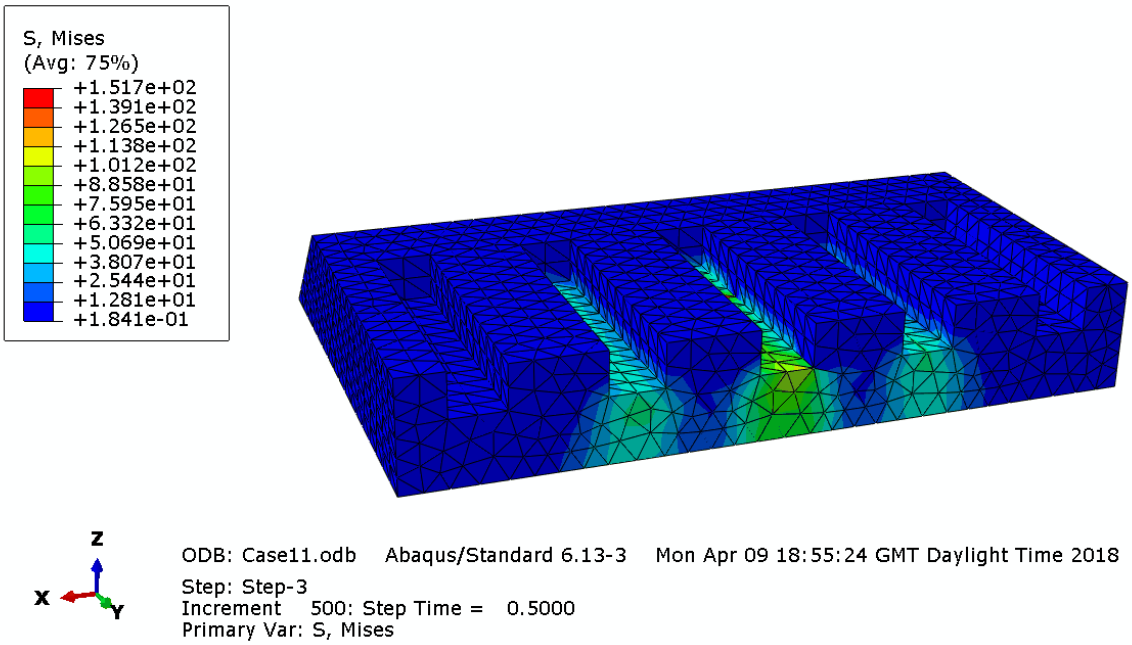

375

376 **Fig. 7.** Von Mises stress distribution for the 5 sleeper model under a 24 t axle load.

377 **Table 4.** Simulation time for different sleeper number (dt = 0.1 s for Step 3)[2].

Sleeper number	CPU time (s)
1 sleeper	56
3 sleepers	127
5 sleepers	255

[2] Computer specifications: Intel(R) Xeon(R) CPU E5-1630 v4 @ 3.70GHz Abaqus and Fortran release: Abaqus 6.13 and Intel Parallel Studio XE2013 (Visual Fortran)

4. Parametric study

A number of simulations are carried out based on the same procedure and setup mentioned in Section 2 and 3 looking at sleeper types, sleeper spacing, and ballast geometry. The role of rail-pad stiffness and USPs is also discussed. Settlement from each case is then plotted against the applied axle load and the stress distributions are shown. The values considered are reported in Table 5 to Table 7. The nominal values are indicated in bold. The total number of variations is 27, varying one parameter at a time. Same Young's modulus (see Table 2) is used for different sleeper types except in case of the wooden sleeper (1.1×10^7 kN/m^2).

Table 5. Track input parameters (nominal values are in bold).

Symbol	Parameter	Values	Justification	N. variations
	Vehicle parameters	22.5t axle load	Freight (UK limit)	**3**
		17t axle load	Intercity passenger	
		12t axle load	Regional passenger	
	Sleeper parameters	See Table 6		**3**
	USP parameters	See Table 7		**4**
L_s	Sleeper spacing, m	0.5/**0.6**/0.7/0.9	Short/typical/long sleeper spacing	**4**
	Rail type	56E1 rail profile		**1**
K_p	Railpad stiffness, kN/mm	50/**200**/500/1000	Very soft/soft/medium/ stiff	**4**
E_f	Foundation stiffness, MN/m^2	10.5	Hard clay	**1**
	Ballast parameters	Based on monotonic triaxial tests	Shi [10], Aingaran [11]	**1**
w	Ballast shoulder width, m	0.2/**0.4**/0.6/.08	Le Pen [14], Kabo [34]	**4**
θ	Ballast slope, deg	30/**45**	Le Pen [14]	**2**
Total number of variations				**27**

Table 6. Sleeper parameters (nominal values are in bold).

	Sleeper height(m)	Sleeper width (m)	Sleeper density (kg/m^3)	Sleeper length (m)
G44 (UK)	**0.2**	**0.24**	**2688**	**2.5**
B90 (Germany)	0.2	0.26	2456	2.6
New oak (UK)	0.15	0.25	923	2.6

Table 7. USP parameters with thickness 20 mm and mass density 500 kg/m^3 [45]

	Young's modulus, (MN/m^2)	Vertical stiffness (kN/mm)	Thickness (mm)
No USPs	-	-	-
Stiff	1000	3000	20
Medium	100	400	20
Soft	10	50	20

4.1 Influence of sleeper type and sleeper spacing

The permanent deformation after one loading cycle varying the applied load and considering different sleeper spacing is presented in Fig. 8. As expected, the increase of sleeper spacing leads to an increase in ballast settlement directly linked to the increased pressure at any single sleeper. The settlement for the longest spacing (0.9 m) is around 6 times higher than the reference value for the case of regional passenger traffic, and the differences decrease with increasing axle tonnage eventually to about 2.5 times for freight. On the contrary, decreasing the sleeper spacing to 0.5 m leads to a significant decrease in plastic deformations around 80% compared to the reference value.

Fig. 9 shows the stress distribution in ballast layer for case with sleeper spacing 0.5 m (the shortest) and 0.9 m (the longest). Similar cone shape stress distribution with angle around 57 degrees can be seen for the two cases. However, unlike the results from sleeper spacing 0.9 m, a clear overlap region can be found from the case with 0.5 m sleeper spacing. Consequently, shorter sleeper spacing provides a more uniform stress distribution which provide better support stiffness, higher confining pressure for a given external load and eventually decrease the permanent deformation.

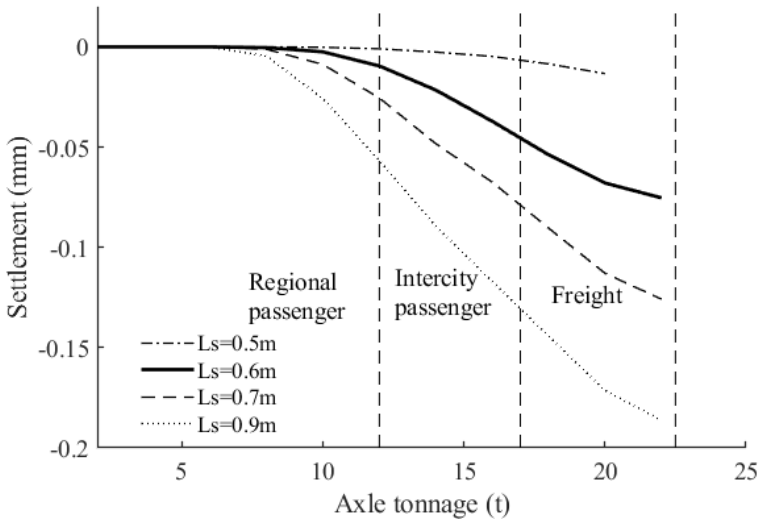

405 **Fig. 8.** Permanent deformation after 1 loading cycle varying the applied load and considering
406 different sleeper spacing values (the reference case is the black thick line).

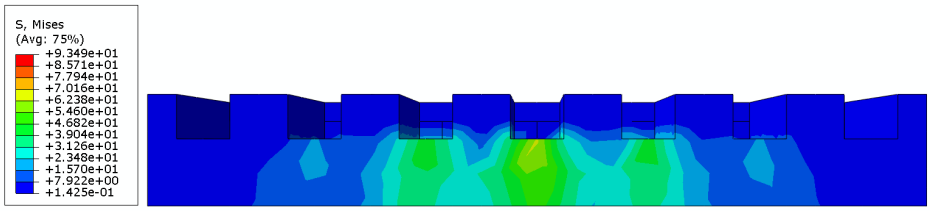

407
408 (a)

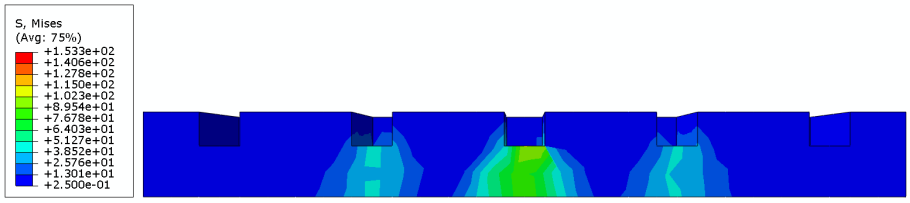

409
410 (b)

411 **Fig. 9.** Stress distribution in the ballast layer with different sleeper spacing (axle tonnage 20 t); (a)
412 sleeper spacing 0.5 m; (b) sleeper spacing 0.9 m.

413 Fig. 10 shows the settlement results with different sleeper types and Fig. 11 the contact pressure
414 between sleeper and ballast before, at peak load (maximum) and after loading. Reductions up to 56%
415 can be found when B90 sleeper is used compared to the reference sleeper. This is due to an increase
416 in the sleeper/ballast contact surface. Although the contact surface of B90 sleeper only increases
417 around 13% compared to the G44 sleeper, a more uniform contact pressure is achieved during the
418 maximum loading and after the loading, as shown in Fig. 11(a), (b). The sleeper made with resilient
419 material (new oak sleeper) offers a higher flexibility reducing pressure overall, as shown in Fig. 11(c).
420 The improvement are similar to B90 sleeper for regional passenger train; however, it tends to decrease
421 with higher axle loads.

422 It is interesting to see how the contact pressure varies during one wheel load passing when different
423 sleeper types are used, as shown in Fig. 11. Two white lines are plotted to indicate the location of two
424 rails.

425 Higher contact pressure can be found near the corner for all cases and a relatively uniform contact
426 pressure distribution can be found for all sleeper types before applying the wheel load. Results near

the corner are not used due to high stress concentration at the boundary between sleeper and ballast continuum. As a result, only the results 0.05 m away from the corner are used for the following discussion.

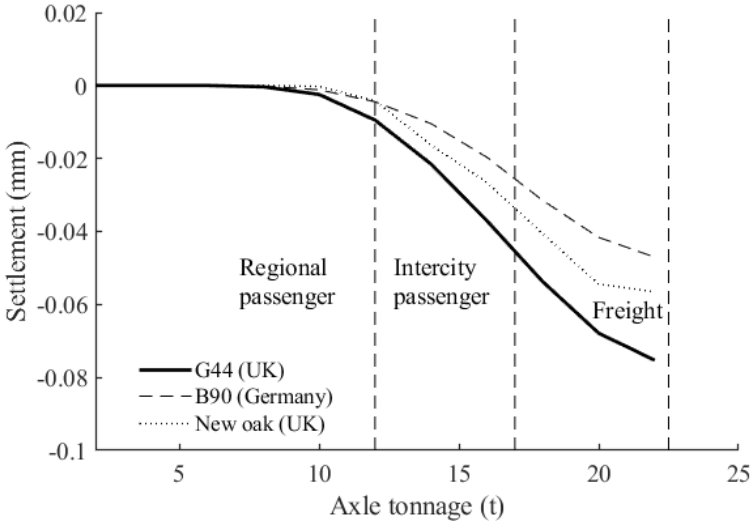

Fig. 10. Permanent deformation after 1 loading cycle varying the applied load and considering different sleeper types (the reference case is the black thick line).

Although the contact pressure is more uniform when concrete sleeper is used during loading, higher contact pressure is found compared to the wooden sleeper. Similar contact pressure pattern can be found for two different concrete sleeper except the contact pressure from B90 is smaller and distributes more uniformly compared to G44 sleeper. On the other hand, the contact pressure from new oak sleeper, which is more resilient, varies significantly while axle load is applied.

Zero contact pressure underneath the rail are found for new oak sleeper after the loading, whereas it is at its maximum during loading, as shown in Fig. 11(c). For the concrete sleeper however, the minimum contact pressure occurs close to the two ends of sleeper instead of underneath the rail. This is due to less deformation and more uniform distribution of contact pressure along the sleeper length that allows the whole sleeper to move downward more constantly during loading, as shown in Fig. 12(a). The granular material tends to move more freely at the side due to lesser boundary restriction when the load is removed, as shown in Fig. 12(b). Displacement tensors for new oak sleeper vary

significantly, as shown in Fig. 13(a), due to significant contact pressure variation and consequently allows the maximum displacement to occur underneath the rail seat after the loading, as shown in Fig. 13(b).

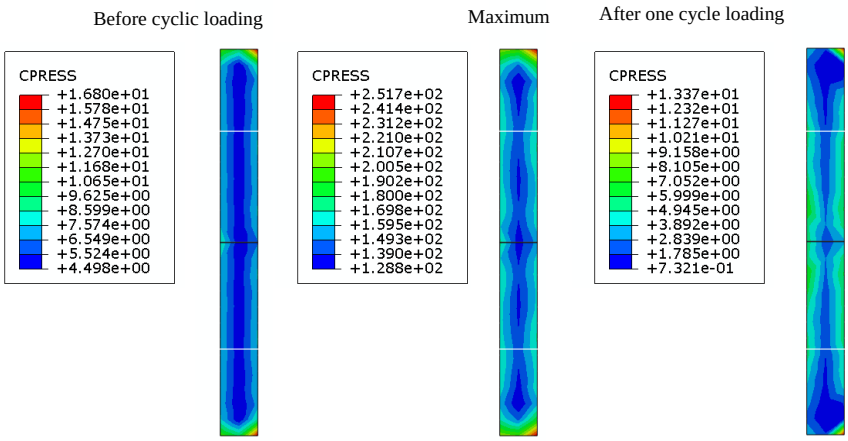

(a)

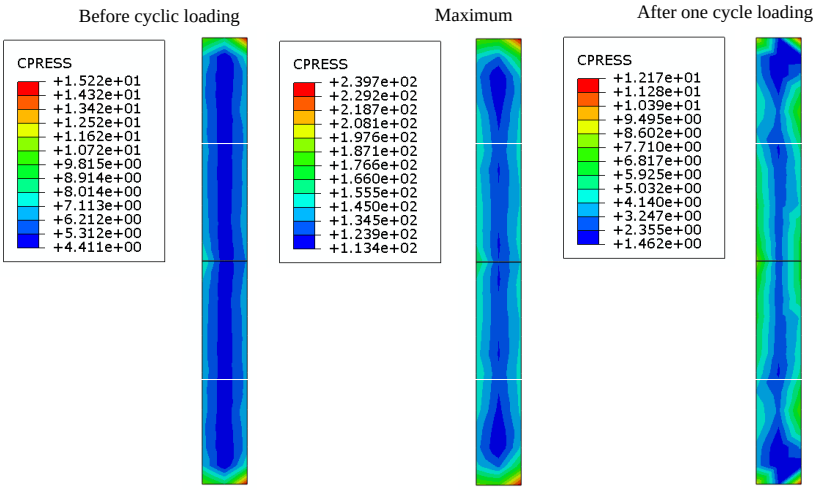

(b)

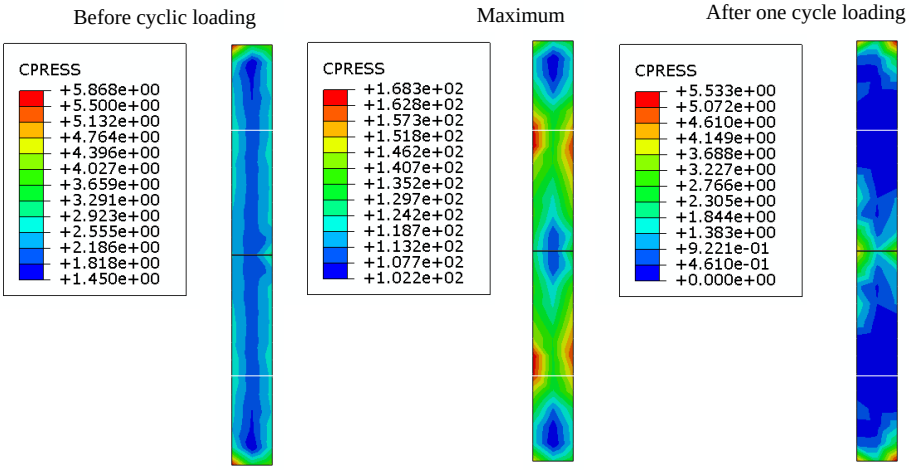

(c)

Fig. 11. Contact pressure variation between sleeper and ballast from different sleeper type during one cycle loading (middle sleeper); (a) G44 sleeper; (b) B90 sleeper; (c) new oak sleeper

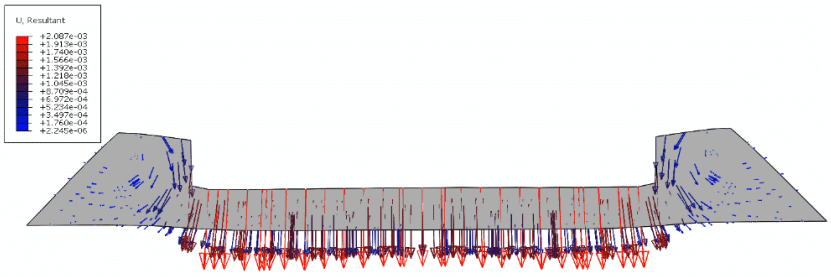

(a)

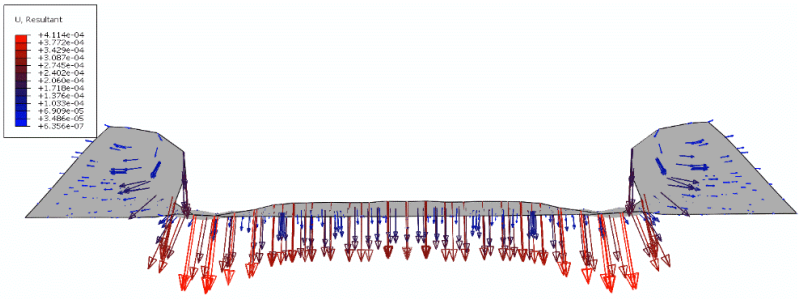

(b)

Fig. 12. Displacement tensor at ballast layer for G44 sleeper; (a) during maximum loading; (b) after the loading (case for 22 axle tonnage).

Although the new oak sleeper shows potential of reducing track settlement (sees Fig. 10), void occurs (location of zero contract pressure) underneath the rail seat, which may accelerate ballast degradation.

As a result, assessment of the sleeper types cannot be based only on settlement analysis but also on the pressure distribution in order to obtain better understanding of the behaviour of ballasted track. Based on the variation of contact pressure, the model has shown the potential for investigating the void generation between ballast and sleeper. The effect of hanging sleeper will eventually occur after a number of cycles and a better understanding of the void variation along the sleeper can be beneficial for improving the ballasted track design or maintenance methodology.

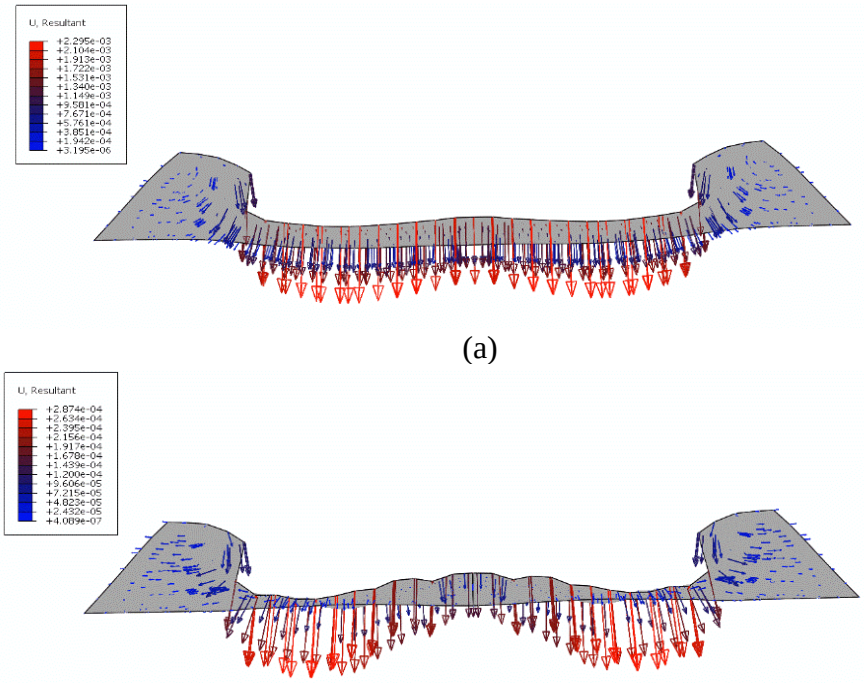

Fig. 13. Displacement tensor at ballast layer for new oak sleeper; (a) during maximum loading; (b) after the loading (case for 22 axle tonnage).

4.2 Influence of ballast geometry

The permanent deformation after one loading cycle varying the applied load and considering different ballast shoulder width and ballast slope is presented in Fig. 14 and Fig. 15, respectively. The results from shallower ballast slope tend to result in smaller settlement at higher axle load due to larger confining pressure contribution. However, only small improvement is found, as shown in Fig. 15. In contrast, more improvement, around 10% reduction compared to the reference value, can be found

from shorter ballast shoulder. The settlement tends to slightly increase when the ballast shoulder width increases at higher axle load and eventually maintain the same after 0.6 m.

Based on the results from the present model, the confining pressure from the ballast layer tends to decrease with increasing ballast shoulder width. The stress tends to distribute wider through the ballast layer when larger ballast shoulder is used and this eventually decrease the confining pressure in the ballast layer and results in larger settlement. Evidence for this phenomena requires further investigation. It has to be noted that the influence of ballast geometry may not be fully captured using the present FE model and additional lab measurements would be required in order to corroborate or not this phenomena.

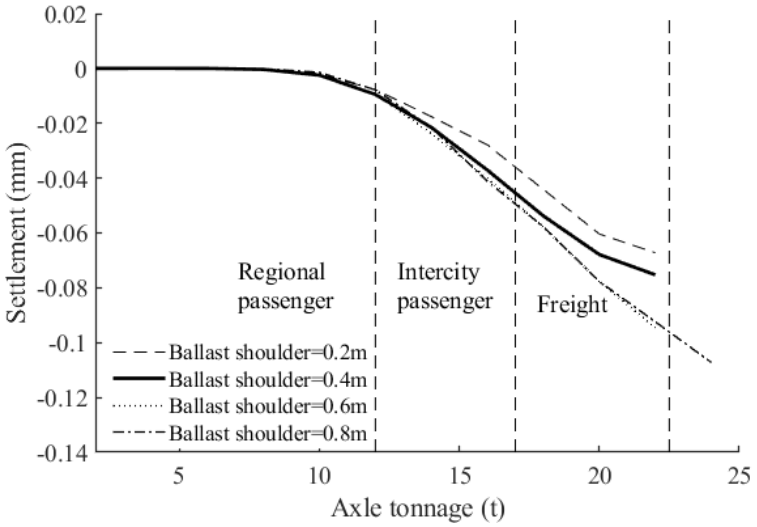

Fig. 14. Permanent deformation after 1 loading cycle varying the applied load and considering different ballast shoulder width (the reference case is the black thick line).

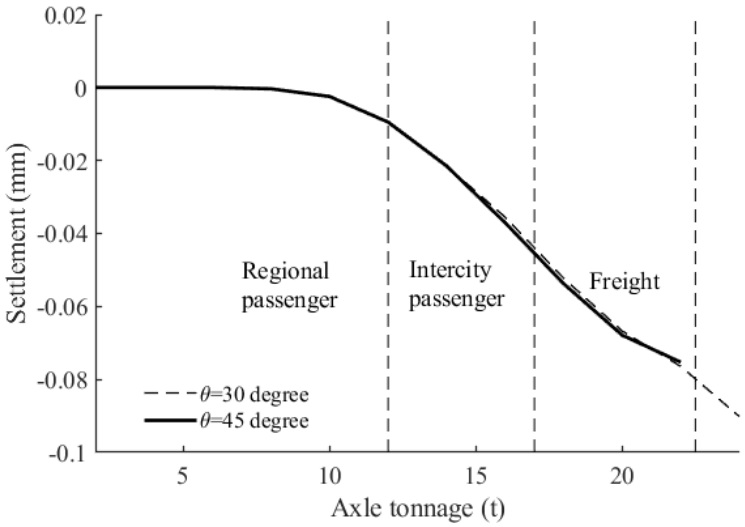

494

495 **Fig. 15.** Permanent deformation after 1 loading cycle varying the applied load and considering
496 different ballast slope (the reference case is the black thick line).

497 **4.3 Influence of rail-pad stiffness**

498 Fig. 16 shows the settlement when different axle tonnage is applied for different rail-pad stiffness.
499 Similar results are found when rail-pad stiffness varies except for soft rail-pad which show around
500 30% and 15% settlement reduction for regional and intercity passenger train and small improvement,
501 around 5%, is found for the freight. This is expected due to the better load distribution over several
502 sleepers and the reduced pressure on ballast, as shown in Fig. 17. However, greater improvement is
503 expected when soft rail-pads are used and when dynamic loads are considered due to the fact that the
504 rail-pad stiffness mainly dominates the dynamic responses at around 200-500 Hz [46,47] and the
505 present study only consider static loads. Consideration of the dynamic load becomes crucial for higher
506 frequency.

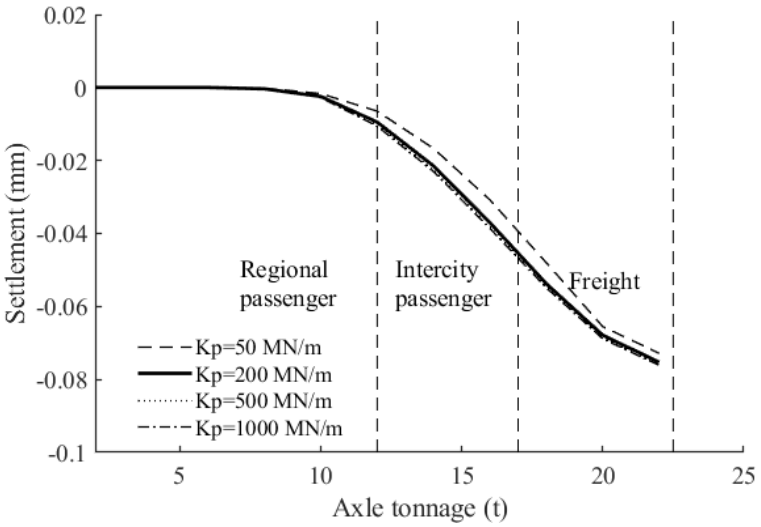

Fig. 16. Permanent deformation after 1 loading cycle varying the applied load and considering different sleeper rail-pad stiffness (the reference case is the black thick line).

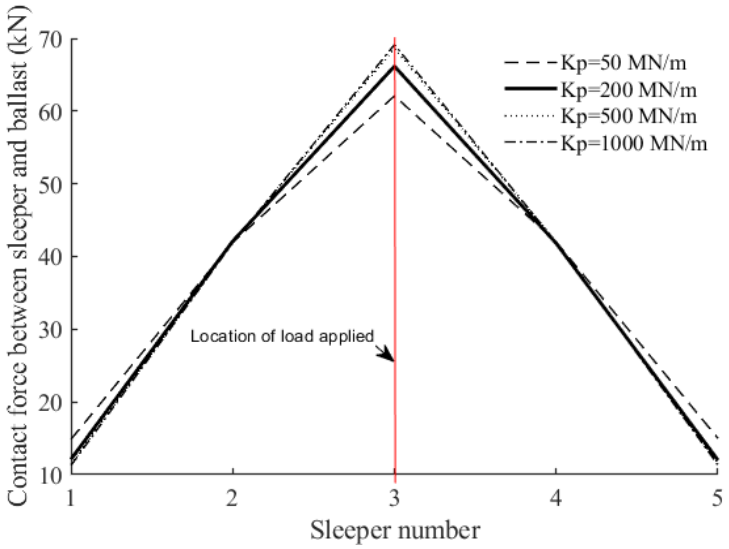

Fig. 17. Sleeper/ballast load distribution along the track

4.4 Influence of the use of USP

Fig. 18 shows the settlement when different axle tonnage is applied with consideration of different USP (stiff, medium, and soft). A very small improvement can be found at higher axle load compared to the results without USP due to more uniform contact pressure. However, the settlement tends to slightly increase when the softer USP is used. Although the use of USP reduces the global track stiffness and allows a wider and more uniform load transfer underneath the sleepers (see Fig. 19), the

confining pressure tends to also decrease which consequently increases the settlement. Same phenomena was also found in experiments. An investigation of different USP was carried out in laboratory and the settlement from the soft USP was found to be larger than the stiff one [48]. The influence of USP may vary depending on the specific USP parameters and track configuration [49,50]. As a result, a further investigation including ballast long-term and dynamic behaviour is required in order to discover the benefit of the use of USP properly. Furthermore, since the current model does not capture the local effect of pressure redistribution with the granular material, DEM modelling maybe more suited to offer a better understanding of the benefit of USPs and capture the actual sleeper/ballast contact surface evolution over time.

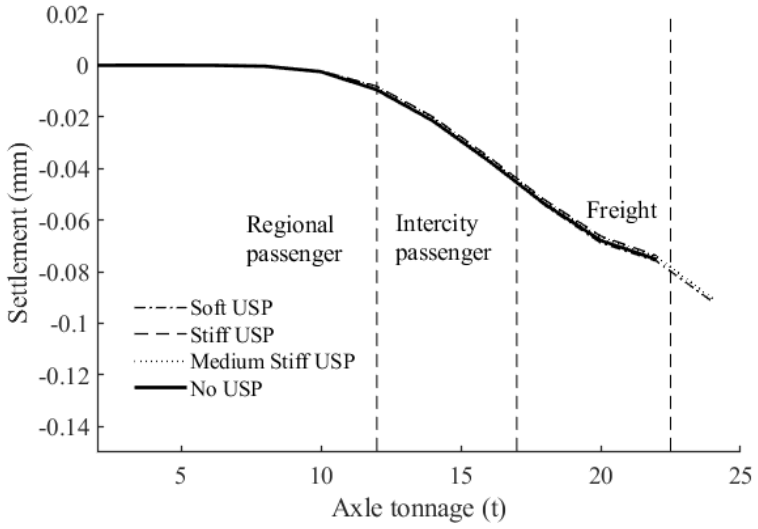

Fig. 18. Permanent deformation after 1 loading cycle varying the applied load and considering different USP stiffness (the reference case is the black thick line).

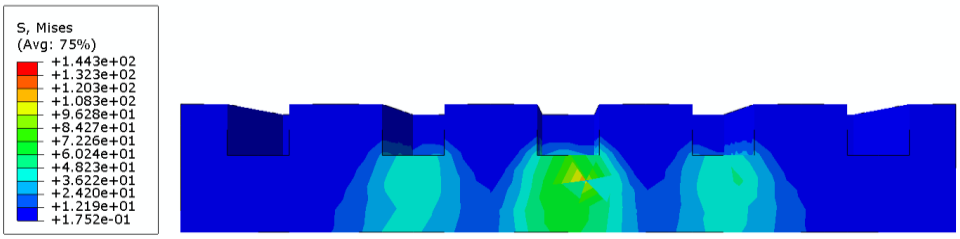

(a)

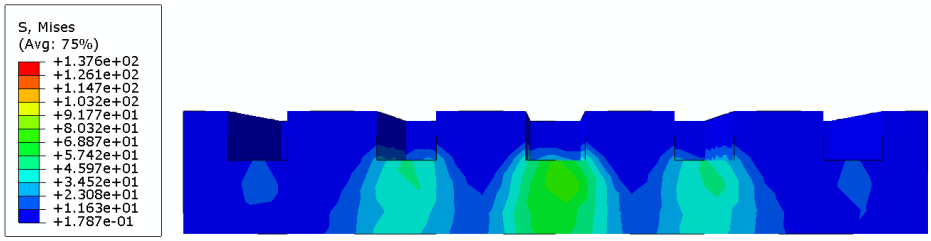

(b)

Fig. 19. Stress distribution in the ballast layer from model using soft USP and without USP (case for 22 axle tonnage); (a) without USP; (b) soft USP

5 Conclusions and future work

A highly efficient and generic ballasted track simulation package BaTrack combining FE software Abaqus, Python and Fortran codes is introduced, which is capable to replicating the mechanical behaviour of the whole track system with different ballast track characteristics. BaTrack includes an advanced ballast material model, capable of capturing ballast nonlinear elasto-plastic behaviour for different confining pressures, and excellent comparative results have been obtained from different triaxial tests and large railway facility measurements. Although long-term behaviour is not considered here beyond the 1st load cycle, the model demonstrates the stress and contact pressure distribution on the ballast layer and has the potential to be used to investigate enhancement techniques for ballasted track as well as for design evaluation purposes. Furthermore, the model has the potential to be used to consider further dynamic loading and long-term behaviour, both of which are planned as future development. Stress and contact pressure distributions are shown to allow a better understanding of how the wheel load transfers through each track component to the ballast layer. Furthermore, the present model has the potential to investigate the void variation between ballast and sleeper based on the contact pressure distribution. Effect of hanging sleeper can be investigated further with consideration of their long-term evolution.

An assessment of boundary effects has been carried out, concluding that a minimum of three to five sleepers are required to accurately capture the settlement, depending on the overall track system stiffness. For example, with no USP and relatively stiff subsoil, three sleepers are sufficient to allow

555 a complete stress distribution, whereas soft soil and the presence of USP would require at least five
556 sleepers.
557 This study shows that sleeper spacing and sleeper types both have a significant potential for reducing
558 track settlement. Up to 80% reduction is found when shorter sleeper spacing is used. Furthermore,
559 around 56% and 13% settlement reductions are found compared to the reference sleeper G44 when
560 B90 (larger sleeper/ballast contact surface) and new oak sleeper (higher flexibility) are used.
561 However, although the general settlement reduces when new oak sleeper is used, voids underneath
562 the rail seat are found, which accelerate the track degradation and does not recommend to be used.
563 Up to around 30% settlement reduction is found when soft rail-pads are used, but higher values may
564 be found when dynamic loads are applied due to the frequency-dependant characteristics. A
565 preliminary study for the use of USP is presented showing that careful selection of USP material is
566 important for ballast settlement. Very small reduction is obtained at higher axle load for stiff and
567 medium stiff USP and the settlement from soft USP slightly increase compared to the results without
568 the USP due to decreased confining pressure in the ballast layer. Further investigation is required in
569 order to obtain better understanding of the benefit of USP.
570 In terms of ballast shape, shallower slope shows small improvement for the ballast settlement due to
571 higher lateral resistance which consequently provides better confining pressure of the ballast layer.
572 On the other hand, around 10% reduction is found compared to the reference ballast shoulder (0.4 m)
573 when smaller ballast shoulder is used and with larger ballast shoulder the settlement tends to increase.
574 This behaviour would appear to contradict common understanding and requires further investigation
575 based on lab tests or using DEMs in order to clarify this phenomena, as the present continuum model
576 may not be able to properly capture the influence of ballast geometry.

577 **Acknowledgement**
578 This work was supported by European project In2Rail (grant agreement No: 635900) and the EPRSC
579 project Track2Future (grant agreement No. EP/M025276/1).

580

581

582 **References**

583 [1] Ishida M, Moto T, Kono A, et al. Influence of Loose Sleeper on Track Dynamics and
584 Bending Fatigue of Rail Welds. Q. Rep. RTRI. 1999;40:80–85.

585 [2] Nielsen; JCO, Igeland A. Vertical dynamic interaction between train and track-influence of
586 wheel and track imperfections. J. Sound Vib. 1995;187:825–839.

587 [3] Lundqvist A, Dahlberg T. Load impact on railway track due to unsupported sleepers. Proc.
588 Inst. Mech. Eng. Part F J. Rail Rapid Transit. 2005;219:67–77.

589 [4] Indraratna B, Ionescu D, Christie HD. Shear Behaviour of Railway Ballast based on Large
590 Scale Triaxial Testing. J. Geotech. Eng. 1998;124:439–449.

591 [5] Indraratna B, Christie D. Effect of confining pressure on the degradation of ballast under
592 cyclic loading. Geotechnique. 2005;55:325–328.

593 [6] Suiker ASJ, Selig ET, Frenkel R. Static and Cyclic Triaxial Testing of Ballast and
594 Subballast. J. Geotech. Geoenvironmental Eng. 2005;771–782.

595 [7] Lackenby J, Indraratna B, McDowell G, et al. Effect of confining pressure on ballast
596 degradation and deformation under cyclic triaxial loading. Géotechnique. 2007;57:527–536.

597 [8] Bian X, Jiang J, Jin W, et al. Cyclic and Postcyclic Triaxial Testing of Ballast and Subballast.
598 J. Mater. Civ. Eng. 2016;1–11.

599 [9] Aursudkij B, McDowell GR, Collop AC. Cyclic loading of railway ballast under triaxial
600 conditions and in a railway test facility. Granul. Matter. 2009;11:391–401.

601 [10] Shi X. Prediction of permanent deformation in railway track. PhD thesis at University of
602 Nottingham; 2009.

603 [11] Aingaran S. Experimental investigation of static and cyclic behaviour of scaled railway
604 ballast and the effect of stress reversal. PhD thesis at University of Southampton; 2014.

[12] Brown SF, Brodrick B V., Thom NH, et al. The Nottingham railway test facility, UK. Proc. ICE - Transp. 2007;160:59–65.

[13] Abadi T, Le Pen L, Zervos A, et al. A Review and Evaluation of Ballast Settlement Models using Results from the Southampton Railway Testing Facility (SRTF). Procedia Eng. 2016;143:999–1006.

[14] Le Pen L, Powrie W. Contribution of base, crib, and shoulder ballast to the lateral sliding resistance of railway track: a geotechnical perspective. Proc. Inst. Mech. Eng. Part F J. Rail Rapid Transit. 2011;225:113–128.

[15] Kennedy JH, Woodward PK, Banimahd M, et al. Railway track performance study using a new testing facility. Proc. ICE - Geotech. Eng. 2012;165:309–319.

[16] Indraratna B, Asce F, Biabani MM, et al. Behavior of Geocell-Reinforced Subballast Subjected to Cyclic Loading in Plane-Strain Condition. J. Geotech. Geoenvironmental Eng. 2015;141:4014081.

[17] Navarro F, Andreu MA, Cámara JL, et al. Short and long term behaviour of high speed lines as determinded in 1:1 scale laboratory tests. 9th World Congr. Railw. Res. 2011.

[18] Zhang X, Zhao C, Zhai W, et al. Investigation of track settlement and ballast degradation in the high-speed railway using a full-scale laboratory test. J. Rail Rapid Transit, Proc. Inst. Mech. Eng. Part F. 2018;0:1–13.

[19] Lim WL, McDowell GR. Discrete element modelling of railway ballast. Granul. Matter. 2005;7:19–29.

[20] Lu M, McDowell GR. The importance of modelling ballast particle shape in the discrete element method. Granul. Matter. 2006;9:69–80.

[21] Lu M, McDowell GR. Discrete element modelling of railway ballast under monotonic and cyclic triaxial loading. Géotechnique. 2010;60:459–467.

[22] Harkness J, Zervos A, Le Pen L, et al. Discrete element simulation of railway ballast:

630 modelling cell pressure effects in triaxial tests. Granul. Matter. 2016;1–13.
631 [23] Ngo NT, Indraratna B, Rujikiatkamjorn C. Stabilization of track substructure with geo-
632 inclusions — experimental evidence and DEM simulation. Int. J. Rail Transp. [Internet].
633 2017;5:63–86. Available from: http://dx.doi.org/10.1080/23248378.2017.1279085.
634 [24] Salim W, Indraratna B. A new elastoplastic constitutive model for coarse granular aggregates
635 incorporating particle breakage. Can. Geotech. J. 2004;41:657–671.
636 [25] Indraratna B, Thakur P, Vinod J, et al. Semiempirical Cyclic Densification Model for Ballast
637 Incorporating Particle Breakage. Int. J. Geomech. 2012;12:260–271.
638 [26] Aubry D, Hujeux JC, Lassoudiere F, et al. A double memory model with multiple
639 mechanisms for cyclic soil behaviour. Geomech., Int. Symp. Num. Mod. Balkema; 1982. p.
640 3–13.
641 [27] Fernandes VA. Numerical analyis of nonlinear soil behavior and heterogeneity effects on
642 railway track response. PhD thesis at École Centrale Paris; 2014.
643 [28] Suiker ASJ, Borst R de. A numerical model for the cyclic deterioration of railway tracks. Int.
644 J. Numer. Methods Eng. 2003;57:441–470.
645 [29] Nguyen K, Villalmanzo DI, Goicolea JM, et al. A computational procedure for prediction of
646 ballasted track profile degradation under railway traffic loading. Proc. Inst. Mech. Eng. Part
647 F J. Rail Rapid Transit. 2016;230:1812–1827.
648 [30] Indraratna B, Salim W, Rujikiatkamjorn C. Advanced Rail Geotechnology - Ballasted Track.
649 CRC Press; 2011.
650 [31] Kalliainen A, Kolisoja P, Nurmikolu A. 3D Finite Element Model as a Tool for Analyzing
651 the Structural Behavior of a Railway Track. Int. Conf. Transp. Geotech. (ICTG 2016).
652 2016;143:820–827.
653 [32] Indraratna B, Salim W, Rujikiatkamjorn C. Development and application of constitutive
654 model for railway ballast. Int. Work. Consitutive Model. Hong Kong; 2007. p. 685–696.

655 [33] Leshchinsky B, Ling H. Effects of Geocell Confinement on Strength and Deformation
656 Behavior of Gravel. J. Geotech. Geoenvironmental Eng. 2013;139:340–352.
657 [34] Kabo E. A numerical study of the lateral ballast resistance in railway tracks. Proc. Inst.
658 Mech. Eng. Part F J. Rail Rapid Transit. 2006;220:425–433.
659 [35] Shih JY, Thompson DJ, Zervos A. The influence of soil nonlinear properties on the
660 track/ground vibration induced by trains running on soft ground. Transp. Geotech.
661 2017;11:1–16.
662 [36] Shih J-Y, Thompson D, Zervos A. Assessment of track-ground coupled vibration induced by
663 high-speed trains. 21st Int. Congr. Sound Vib. 2014.
664 [37] Shih J-Y. Models for vehicle/track/ground interaction in the time domain. PhD thesis at
665 University of Southampton; 2017.
666 [38] Abaqus Analysis User's Guide 6.13.
667 [39] Biabani MM, Indraratna B, Ngo NT. Modelling of geocell-reinforced subballast subjected to
668 cyclic loading. Geotext. Geomembranes. 2016;44:489–503.
669 [40] Anderson WF, Fair P. Behavior of Railroad Ballast under Monotonic and Cyclic Loading. J.
670 Geotech. Geoenvironmental Eng. 2008;134:316–327.
671 [41] Hicks RG, Monismith CL. Factors influencing the resilient response of granular materials.
672 Highw. Res. Rec. 1971;345:15–31.
673 [42] Wu W, Owino J. Applying Periodic Boundary Conditions in Finite Element Analysis.
674 Simulia Community Conf. 2014;707–719.
675 [43] Le Pen L. Track behaviour: the importance of the sleeper to ballast interface. PhD thesis at
676 University of Southampton; 2008.
677 [44] Bowles JE. Foundation Analysis and Design. Third Edit. Mcgraw-Hill, Inc.: USA.; 1982.
678 [45] Witt S. The Influence of Under Sleeper Pads on Railway Track Dynamics. Proc. Linköping
679 Univ. 2008.

[46] Thompson DJ. Railway Noise and Vibration, Mechanisms, Modelling and Means of Control. Oxford: Oxford Elsevier Ltd; 2009.

[47] Shih J-Y, Kostovasilis D, Bezin Y, et al. Modelling options for ballast track dynamics. 24th Int. Congr. Sound Vib. ICSV 2017. 2017.

[48] Safari Baghsorkhi M, Laryea S, McDowell G, et al. An investigation of railway sleeper sections and under sleeper pads using a box test apparatus. Proc. Inst. Mech. Eng. Part F J. Rail Rapid Transit. 2016;230:1722–1734.

[49] Jayasuriya C, Indraratna B, Nimbalkar S. Analysis of the Performance of Under Sleeper Pads- A Critical Review. Int. Conf. Geotech. Eng. Colombo, Sri Lanka; 2015. p. 601–604.

[50] Schneider P, Bolmsvik R, Nielsen JCO. In situ performance of a ballasted railway. J. Rail Rapid Transit, Proc. Inst. Mech. Eng. Part F. 2010;225:299–309.